Copy 5
RM L54G27

NACA RM L54G27

NACA

RESEARCH MEMORANDUM

FOR REFERENCE

NOT TO BE TAKEN FROM THIS ROOM

LOW-SPEED MEASUREMENTS OF ROLLING AND YAWING STABILITY DERIVATIVES OF A 60° DELTA-WING MODEL

By Joseph L. Johnson, Jr.

Langley Aeronautical Laboratory
Langley Field, Va.

CLASSIFICATION CHANGED

To UNCLASSIFIED

AIRCRAFT COPY

DEC 28 1954

LANGLEY AERONAUTICAL LABORATORY
LIBRARY, NACA
LANGLEY FIELD, VIRGINIA

By authority of RN-127 Date May 16, 1958

CLASSIFIED DOCUMENT

This material contains information affecting the National Defense of the United States within the meaning of the espionage laws, Title 18, U.S.C., Secs. 793 and 794, the transmission or revelation of which in any manner to an unauthorized person is prohibited by law.

NATIONAL ADVISORY COMMITTEE
FOR AERONAUTICS

WASHINGTON

December 27, 1954

NATIONAL ADVISORY COMMITTEE FOR AERONAUTICS

RESEARCH MEMORANDUM

LOW-SPEED MEASUREMENTS OF ROLLING AND YAWING STABILITY DERIVATIVES OF A 60° DELTA-WING MODEL

By Joseph L. Johnson, Jr.

SUMMARY

An investigation has been made in the Langley free-flight tunnel to determine the low-speed rolling and yawing stability derivatives of a 60° delta-wing model from 0° to 30° angle of attack. The derivatives were measured by the free-to-damp oscillation technique and by the steady-roll technique. The results of the investigation showed that the damping-in-yaw parameter $C_{n_r} - C_{n_{\dot{\beta}}}$ determined from free-to-damp oscillation tests was much larger in the high angle-of-attack range than the value of the damping-in-yaw parameter C_{n_r} determined for a similar model by the yawing-flow technique. The damping-in-roll parameter C_{l_p} decreased with increasing angle of attack and became approximately zero at an angle of attack of 30°.

INTRODUCTION

Results of recent unpublished lateral stability calculations based on semiempirical estimates of the stability derivatives have indicated considerable differences in the dynamic lateral stability characteristics from those determined from flight tests of airplanes with highly swept wings. The difference between the experimental and calculated results is believed to be caused by possible inaccuracies in the estimated values of some of the yawing and rolling stability derivatives used in the calculations. Because of the need for such information, tests have been made to measure some of the rolling and yawing stability derivatives of a model representative of a jet-propelled, fighter-type airplane with 60° delta wing and tail surfaces.

The present investigation consisted of free-to-damp oscillation tests to determine the damping-in-yaw derivative $C_{n_r} - C_{n_{\dot{\beta}}}$ and damping-in-roll derivative C_{l_p} over an angle-of-attack range from 0°

to 30°. A few steady-roll tests were also made to determine C_{l_p} and the yawing-moment-due-to-rolling derivative C_{n_p}. In addition, free-to-damp oscillation tests were made to determine the effect on the damping in yaw of leading-edge slats.

SYMBOLS

Unless otherwise noted, all stability parameters and coefficients are referred to the stability system of axes originating at a center-of-gravity position of 30 percent of the mean aerodynamic chord and located on the longitudinal body axis. (See fig. 1.)

S	wing area, sq ft
$\bar{c}$	mean aerodynamic chord, ft
V	airspeed, ft/sec
b	wing span, ft
q	dynamic pressure, lb/sq ft
ρ	air density, slug/cu ft
β	angle of sideslip, deg
ψ	angle of yaw, deg
ϕ	angle of bank, deg
α	angle of attack, deg
θ	angle of pitch, deg; $\theta = \alpha$ when ψ and ϕ are zero
X	longitudinal force, lb
Y	lateral force, lb
Z	normal force, lb
M	pitching moment, lb-ft
N	yawing moment, lb-ft

L rolling moment, lb-ft

C_L lift coefficient, Lift/qS

C_D drag coefficient, Drag/qS

C_m pitching-moment coefficient, Pitching moment/qS$\bar{c}$

C_Y lateral-force coefficient, Lateral force/qS

C_n yawing-moment coefficient, Yawing moment/qSb

C_l rolling-moment coefficient, Rolling moment/qSb

$C_{Y_\beta} = \frac{\partial C_Y}{\partial \beta}$ per deg

$C_{n_\beta} = \frac{\partial C_n}{\partial \beta}$ per deg

$C_{l_\beta} = \frac{\partial C_l}{\partial \beta}$ per deg

$C_{n_p} = \frac{\partial C_n}{\partial \frac{pb}{2V}}$ per radian

$C_{l_p} = \frac{\partial C_l}{\partial \frac{pb}{2V}}$ per radian

$C_{n_r} = \frac{\partial C_n}{\partial \frac{rb}{2V}}$ per radian

$C_{n_{\dot{\beta}}} = \frac{\partial C_n}{\partial \frac{\dot{\beta} b}{2V}}$ per radian

$C_{l_{\dot{\beta}}} = \frac{\partial C_l}{\partial \frac{\dot{\beta} b}{2V}}$ per radian

p rolling angular velocity, radians/sec

r yawing angular velocity, radians/sec

$\dot{\beta}$ rate of change of angle of sideslip, radians/sec

δ_e elevator deflection perpendicular to hinge line (elevons deflected together for elevator control), deg

APPARATUS AND MODEL

The free-to-damp oscillation tests were made in the Langley free-flight tunnel on an oscillation apparatus which permitted the model to have only one degree of freedom at a time - either freedom in yaw or freedom in roll. For the steady roll force tests, an internal strain-gage balance was used to record the forces and moments as the model was forced to roll at a constant rate. The test apparatus used in this investigation was the same as that used in reference 1 except for a modification which permitted tests in this investigation about the stability axes instead of the body axes. This modification consisted of a circular track to which was attached the model and sting. The attachment point of the sting to the track was adjustable to allow for changes in angle of attack. A drawing of the model and test apparatus used in this investigation is shown in figure 2 and a general description of the oscillation apparatus is given in reference 1.

A three-view drawing of the model used in the investigation is presented in figure 3 and the dimensional characteristics of the model are given in table I. The model has a 60° delta wing of aspect ratio 2.2 and a 60° delta vertical tail.

TESTS

Free-to-damp oscillation tests were made by the method described in reference 1 to determine the values of the damping-in-yaw and damping-in-roll parameters over an angle-of-attack range from 0° to 30° for the model with vertical tail off and on. A few steady-roll tests were also made to determine C_{l_p} and C_{n_p} over the angle-of-attack range for the model with vertical tail off and on. In addition, free-to-damp oscillation tests were made to determine the effect on damping in yaw of leading-edge slats. All the oscillation tests were made at a frequency of about 1 cycle per second.

All the tests were made at a dynamic pressure of 3.80 pounds per square foot which corresponds to an airspeed of approximately 57.3 feet

per second and to an effective Reynolds number of 850,000 based on the mean aerodynamic chord of 2.32 feet.

No attempt was made in this investigation to determine the effect of frequency or changes in amplitude of the oscillation on the lateral damping. For all the oscillation tests the model was displaced in yaw or roll about 30° before being released and allowed to damp to 0° amplitude. The envelopes of the oscillations were plotted on semilogarithmic paper and were found to be fairly linear through the amplitude range investigated except for small amplitudes where the tunnel turbulence caused the data to be erratic. Because of the nonlinearity of the data at the small amplitudes, the logarithmic decrements or damping factors used to determine the damping derivatives of this investigation were obtained from the slope of the envelope curves for amplitudes above approximately ±2° or ±3°.

RESULTS AND DISCUSSION

For the convenience of the reader, static data are presented in figures 4 and 5. The data of figure 4 show the static longitudinal characteristics of the model in the clean configuration. The data of figure 5 show the static lateral stability parameters for the model with leading-edge slats off and on and with the vertical tail off and on.

Damping in Yaw

Clean configuration.- The results of the free-to-damp oscillation tests in yaw presented in figure 6(a) show that the model in the clean configuration had positive damping in yaw (negative value of $C_{n_r} - C_{n_{\dot{\beta}}}$) at an angle of attack of 0° and that the damping increased rapidly with increasing angle of attack. The damping in yaw contributed by the vertical tail was about constant over the low and moderate angle-of-attack range. At an angle of attack of 30°, however, the tail contribution was almost twice that at low angles of attack. Also, presented in figure 6(a) are values of C_{n_r} from reference 2 determined by the yawing-flow technique for a 60° delta-wing model similar in some respects to the subject model. At the higher angles of attack the values of C_{n_r} are much lower than the values of $C_{n_r} - C_{n_{\dot{\beta}}}$. These results appear to be similar to unpublished results obtained in the Langley stability tunnel on a model having a 45° sweptback wing where it was found that C_{n_r} determined from yawing-flow tests was much lower at the higher angles of attack than $C_{n_r} - C_{n_{\dot{\beta}}}$ determined from oscillation tests.

The rapid increase in $C_{n_r} - C_{n_{\dot{\beta}}}$ for the wing-fuselage combination at the high angles of attack is not completely understood but it is believed to be associated with the rapid increase in static directional instability of the wing-fuselage combination (fig. 5). It is possible that, because of the lag in the buildup and decay of the load on the wing as the model oscillates in yaw, large positive values of $C_{n_{\dot{\beta}}}$ (increased damping) might be obtained at angles of attack where the model has large negative values of C_{n_β}.

The increase in the tail contribution to $C_{n_r} - C_{n_{\dot{\beta}}}$ at the high angles of attack is at least partly attributed to the vortex flow over the rear portion of the model. Some indication of the physical nature of this vortex flow is shown in the tuft-grid studies of reference 3. These studies showed that a delta-wing model oscillating in yaw had trailing vortices and resulting sidewash fields generally similar to those found in tuft-grid studies of a model in static tests (ref. 4). In both cases, the vortex flow from the leading wing moved inboard and created a sidewash over the rear portion of the model. In the case of the oscillation tests, this sidewash lagged behind the motion of the model so that at any instant the vertical tail was at a higher angle of attack than it would have been with no sidewash present. The resulting increase in the contribution of the vertical tail to the damping in yaw is represented by the term $C_{n_{\dot{\beta}}}$.

Unpublished lateral stability calculations made for the 60° delta-wing model indicated an unstable Dutch roll oscillation at high angles of attack. When these calculations were repeated using the measured values of $C_{n_r} - C_{n_{\dot{\beta}}}$ shown in figure 6 instead of the much smaller estimated values of C_{n_r}, the calculated Dutch roll oscillation was stable at all angles of attack. These results emphasize the necessity for using the oscillation damping-in-yaw parameter for calculations of Dutch roll stability, particularly at high angles of attack where the term $C_{n_{\dot{\beta}}}$ becomes large.

Slats on.- The data of figure 6(b) show that the addition of the leading-edge slats to the model with vertical tail off had little effect on the damping-in-yaw parameter. For the vertical tail-on configuration, however, the addition of the slats reduced the damping in yaw at the higher angles of attack to the extent that the model was more heavily damped with vertical tail off than vertical tail on.

Damping in Roll

The results of steady-roll tests to determine C_{l_p} and C_{n_p} are presented in figure 7(a) and the results of free-to-damp oscillation

tests to determine C_{l_p} are presented in figure 7(b). The C_{l_p} data from the two types of tests are in good agreement and show a gradual decrease in damping in roll with increasing angle of attack. At the highest angles of attack, the tail-on configuration had slightly less damping in roll than the tail-off configuration.

The model had very low values of C_{n_p} over the low and moderate angle-of-attack range with the vertical tail off or on. In the higher angle-of-attack range, C_{n_p} with tail off increased rapidly to large negative values and there was also a large negative increment contributed by the vertical tail.

In flight tests of the 60° delta-wing model in the Langley free-flight tunnel the observed damping-in-roll characteristics of the model at high angles of attack appeared to be good - a result which, at first glance, appeared to be in disagreement with the C_{l_p} data of figure 7. This apparent discrepancy can be explained by the damping-in-roll data for this same model measured about the body axis which is presented in reference 1. These data are shown in figure 8, together with the data measured about the stability axis from figure 7. With increasing angle of attack the damping in roll measured about the body axis increased rather than decreased and, at an angle of attack of 30°, the damping in roll was about twice as large as that at 0° angle of attack. This increase in damping with increasing angle of attack can be partly explained by using $C_{n_r} - C_{n_{\dot{\beta}}}$ instead of C_{n_r} in the geometrical relationship of reference 5 for transferring rotary derivatives from the stability axes to the body axes. A large part of this increase in damping, however, appears to be associated with the fact that angular displacements in roll about the body axis produce sideslipping. As the model oscillates in roll, the lag in the buildup or decay of the rolling moment on the wing probably produces additional damping in roll which is represented by the term $C_{l_{\dot{\beta}}} \sin \theta$. (See ref. 1.) This variation of $C_{l_p} + C_{l_{\dot{\beta}}} \sin \theta$ with angle of attack appears to be in much better agreement with the pilots' impressions of the damping in roll of the model in the flight tests. Analysis indicates that this is a logical result since the pilots' impressions of the damping in roll at high angles of attack always appears to be obtained from the rolling motions about the body axis rather than the stability axis. It is believed that this result will also apply for the full-scale airplane in that the pilot will sense the damping in roll about the body axis rather than the stability axis.

CONCLUDING REMARKS

An investigation has been conducted in the Langley free-flight tunnel to determine the low-speed rolling and yawing stability derivatives

of a 60° delta-wing model. The results of the investigation showed that the damping-in-yaw parameter $C_{n_r} - C_{n_{\dot{\beta}}}$ determined from free-to-damp oscillation tests was much larger in the high angle-of-attack range than the value of the damping-in-yaw parameter C_{n_r} determined for a similar model by the yawing-flow technique. The damping-in-roll parameter C_{l_p} decreased with increasing angle of attack and became approximately zero at an angle of attack of 30°.

Langley Aeronautical Laboratory,
National Advisory Committee for Aeronautics,
Langley Field, Va., July 7, 1954.

REFERENCES

1. Hewes, Donald E.: Low-Speed Measurement of Static Stability and Damping Derivatives of a 60° Delta-Wing Model for Angles of Attack of 0° to 90°. NACA RM L54G22a, 1954.

2. Goodman, Alex: Effect of Various Outboard and Central Fins on Low-Speed Yawing Stability Derivatives of a 60° Delta-Wing Model. NACA RM L50E12a, 1950.

3. Bird, John D., and Riley, Donald R.: Some Experiments on Visualization of Flow Fields Behind Low-Aspect-Ratio Wings by Means of a Tuft Grid. NACA TN 2674, 1952.

4. Johnson, Joseph L., Jr.: A Study of the Flow Field Behind the Triangular Horizontal Tail of a Canard Airplane at Approximately the Vertical-Tail Location by Means of a Tuft Grid. NACA RM L52H11, 1952.

5. Jones, B. Melvill: Dynamics of the Aeroplane. The Asymmetric or Lateral Moments. Vol. V of Aerodynamic Theory, div. N, ch. III, sec. 21, W. F. Durand, ed., Julius Springer (Berlin), 1935, pp. 71-72.

TABLE I.- DIMENSIONAL CHARACTERISTICS OF THE 60° DELTA-WING MODEL TESTED IN THE LANGLEY FREE-FLIGHT TUNNEL

Wing:	
Airfoil	NACA 0004-65 modified
Area, sq ft	6.6150
Span, ft	3.813
Aspect ratio	2.198
Root chord, ft	3.469
Tip chord, ft	0
$\bar{c}$, ft	2.322
Longitudinal distance from leading-edge root chord to leading edge of $\bar{c}$, ft	1.101
Sweepback of leading edge, deg	60
Sweepforward of trailing edge, deg	5
Dihedral, deg	0
Incidence, deg	0
Slats:	
Span, percent wing span (two)	31.7
Chord, ft	0.136
Elevons:	
Area behind hinge line, percent wing area (two)	10.12
Span, percent wing span (two)	69.0
Root chord, ft	0.315
Tip chord, ft	0.204
Vertical tail:	
Airfoil section	NACA 0004-65 modified
Area, sq ft	0.682
Span, ft	0.866
Aspect ratio	1.10
Sweepback of leading edge, deg	60
Longitudinal distance from center-of-gravity location to center of pressure of vertical tail, ft	1.26

[redacted]

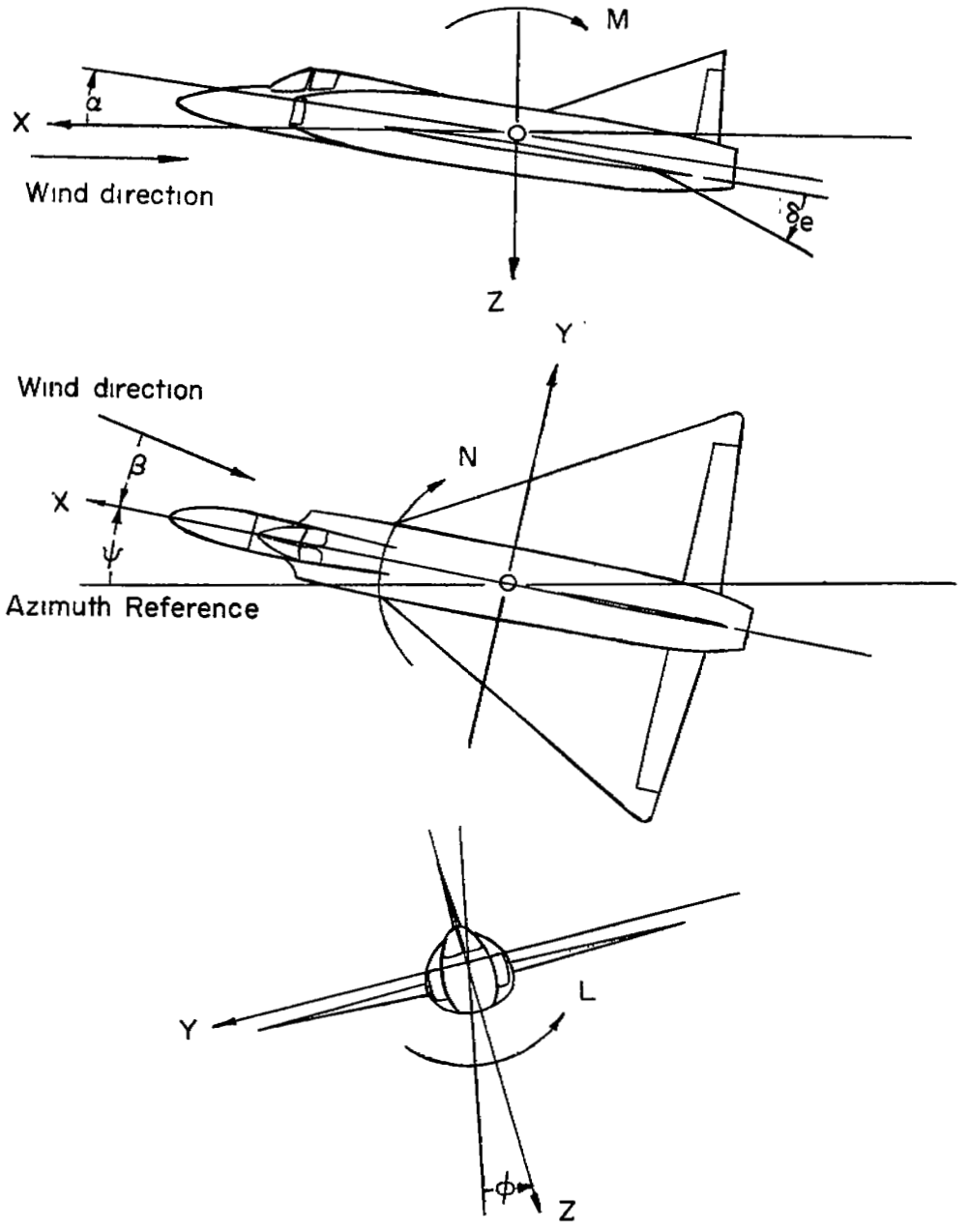

Figure 1.- The stability system of axes. Arrows indicate positive directions of moments, forces, and angles. This system of axes is defined as an orthogonal system having the origin at the center of gravity and in which the Z-axis is in the plane of symmetry and perpendicular to the relative wind, the X-axis is in the plane of symmetry and perpendicular to the Z-axis, and the Y-axis is perpendicular to the plane of symmetry. At a constant angle of attack, these axes are fixed in the airplane.

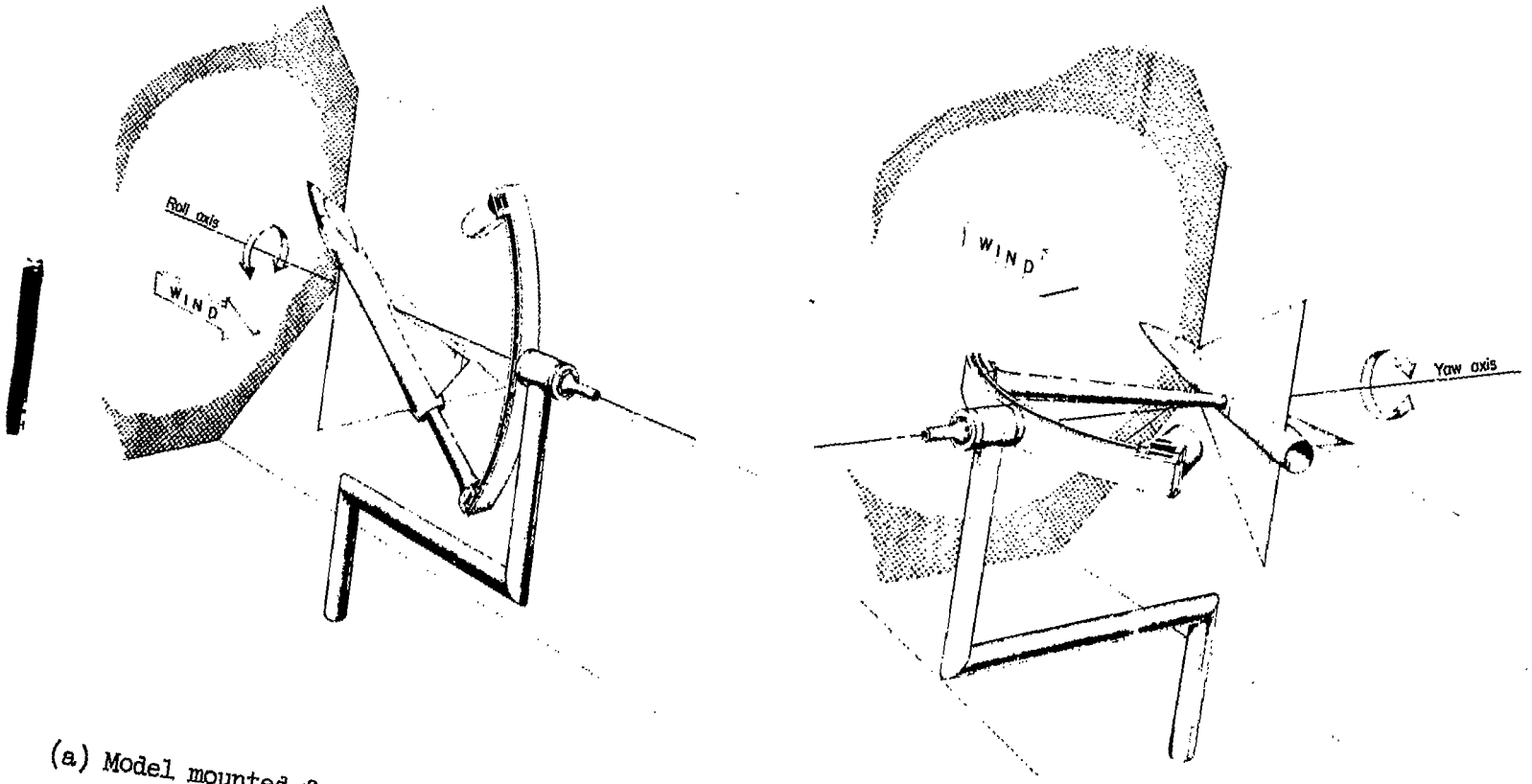

(a) Model mounted for damping-in-roll tests.

(b) Model mounted for damping-in-yaw tests.

L-85594

Figure 2.- Schematic drawings of test setup.

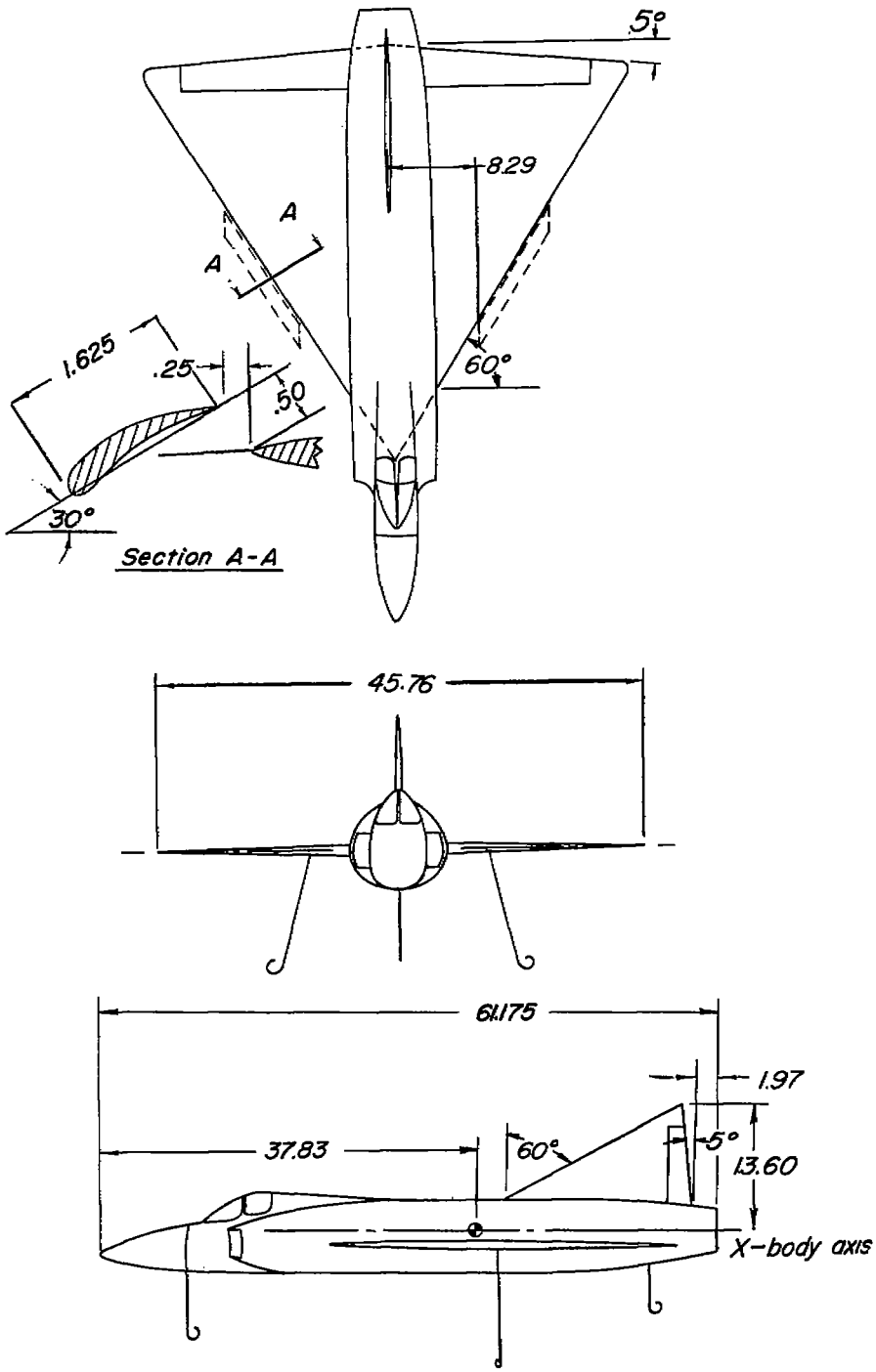

Figure 3.- Three-view drawing of the model tested in the Langley free-flight tunnel. All dimensions are in inches.

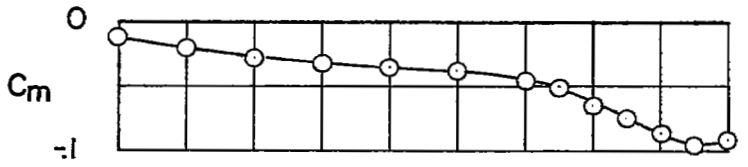

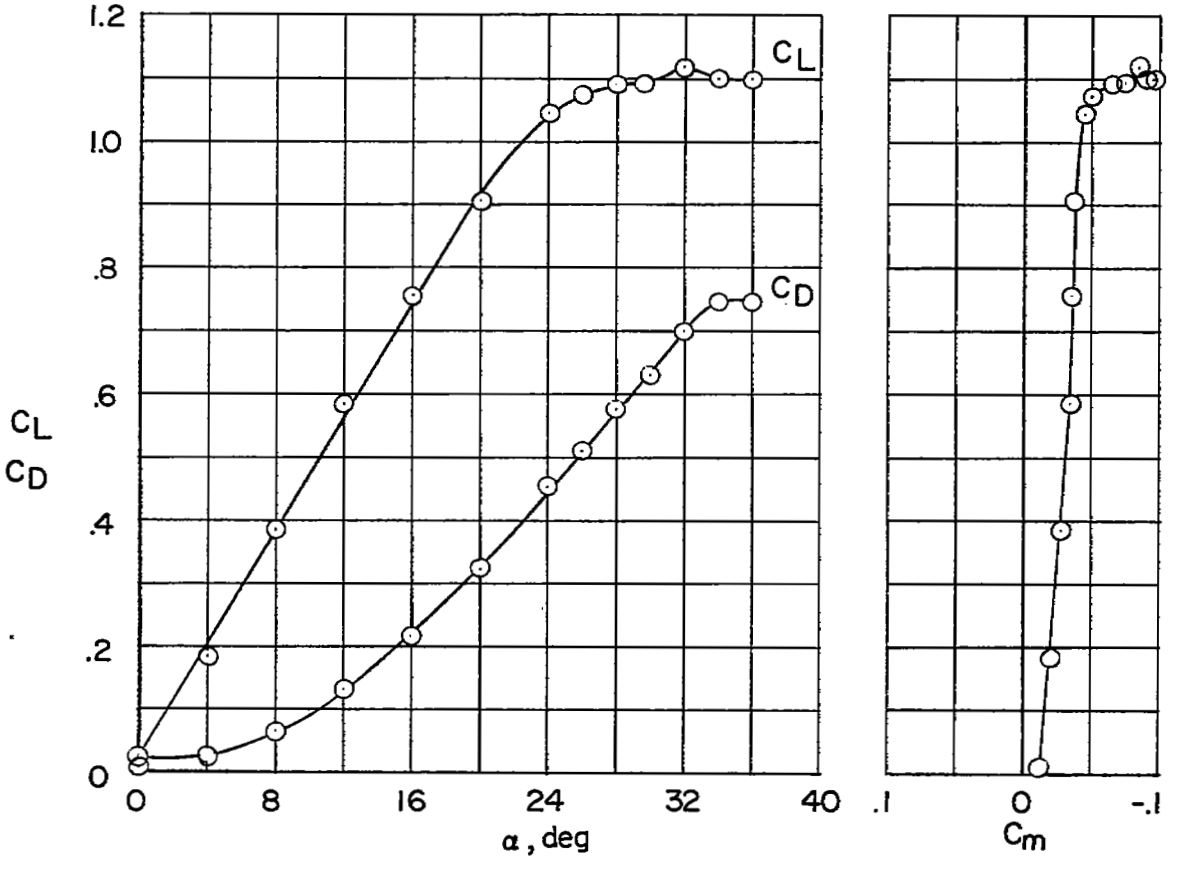

Figure 4.- Longitudinal characteristics of the model. $\delta_e = 0^o$.

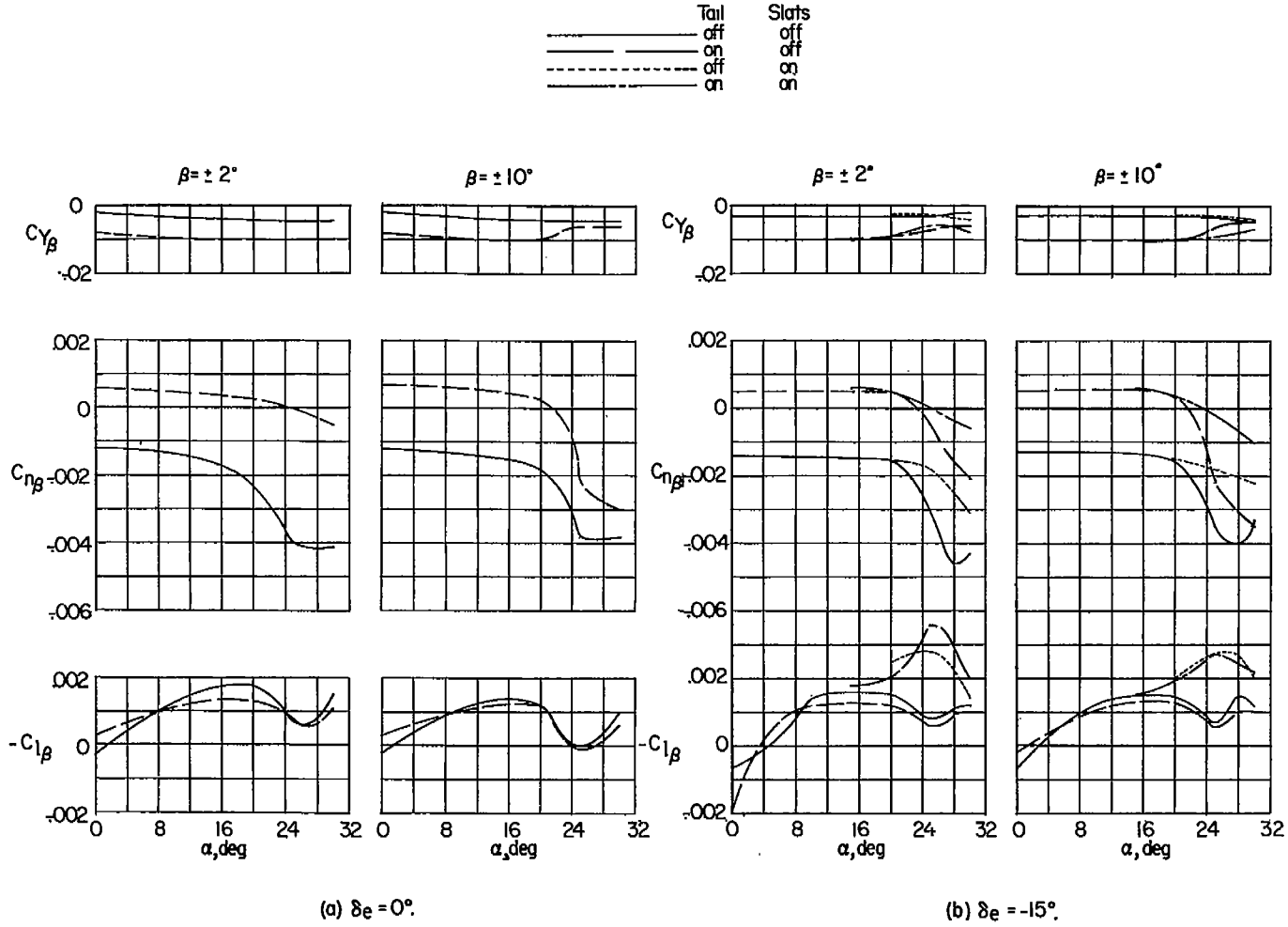

(a) $\delta_e = 0°$.

(b) $\delta_e = -15°$.

Figure 5.- Static lateral stability parameters of the model. Derivatives determined as follows:

$$C_{n_\beta} = \frac{(C_n)_{\beta=2^o} - (C_n)_{\beta=-2^o}}{4}, \quad C_{n_\beta} = \frac{(C_n)_{\beta=10^o} - (C_n)_{\beta=-10^o}}{20}, \text{ etc.}$$

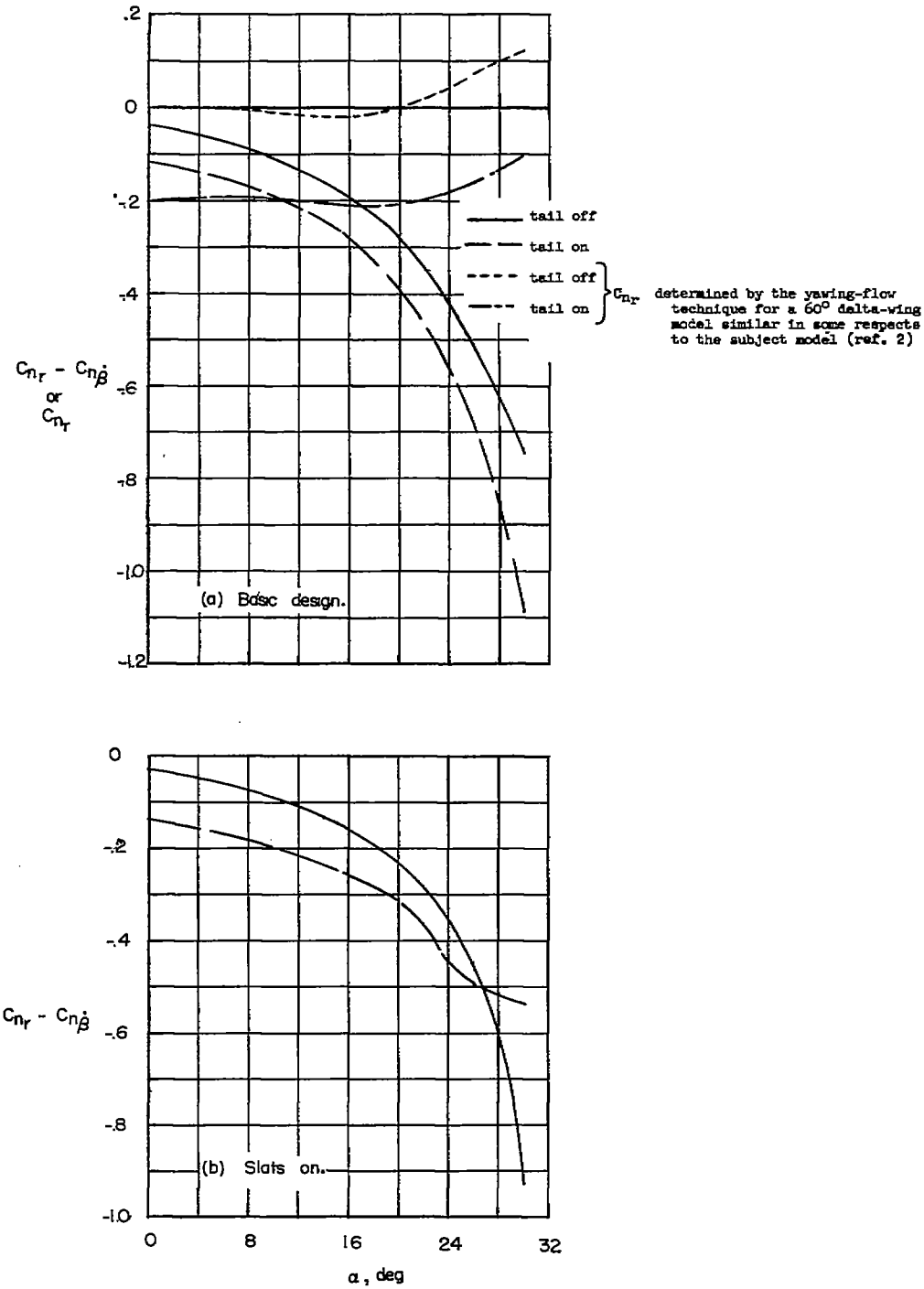

Figure 6.- Damping-in-yaw derivatives. $\delta_e = 0°$.

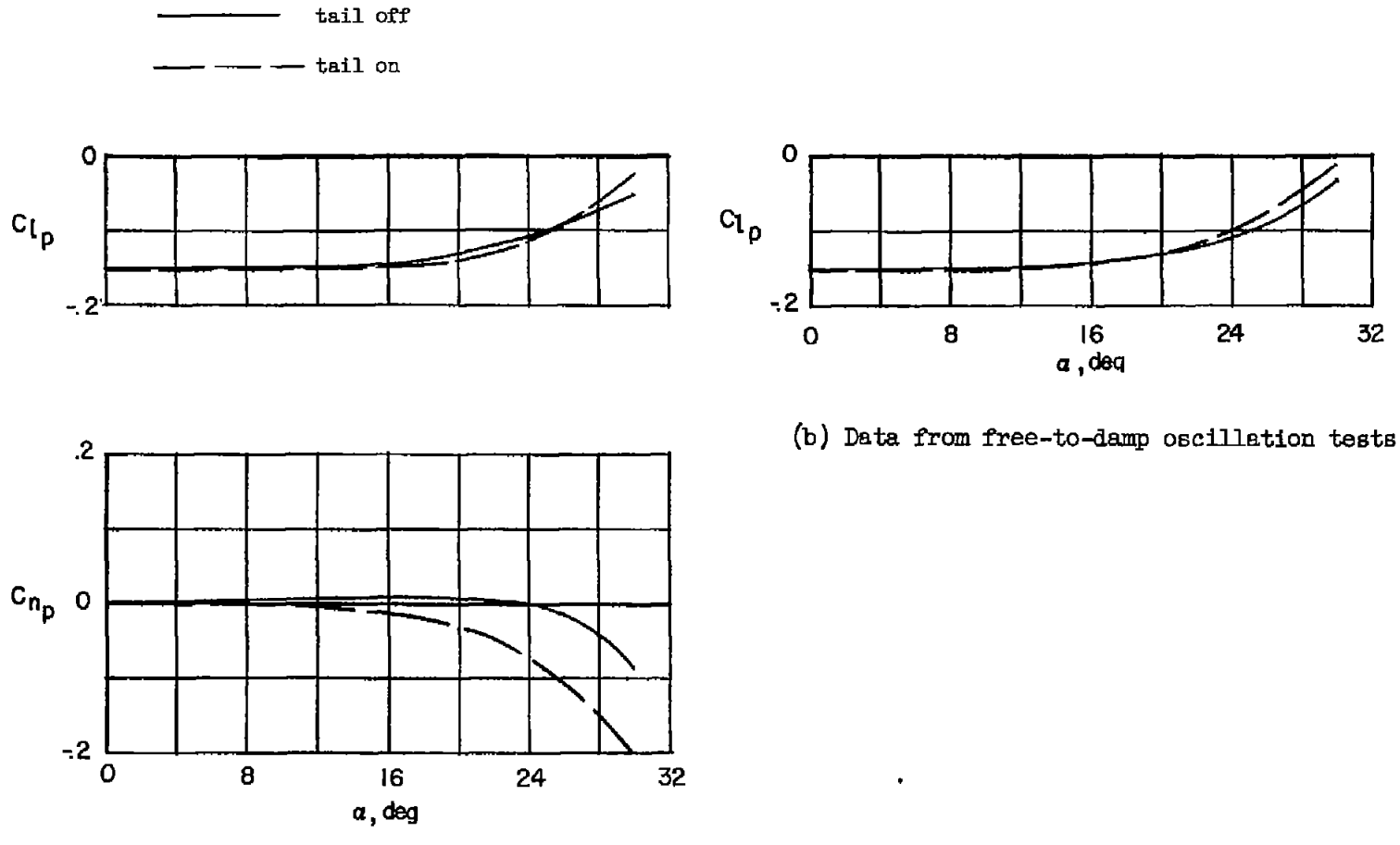

(a) Data from steady-roll tests.

(b) Data from free-to-damp oscillation tests.

Figure 7.- Rolling stability derivatives of the model. $\delta_e = 0^o$.

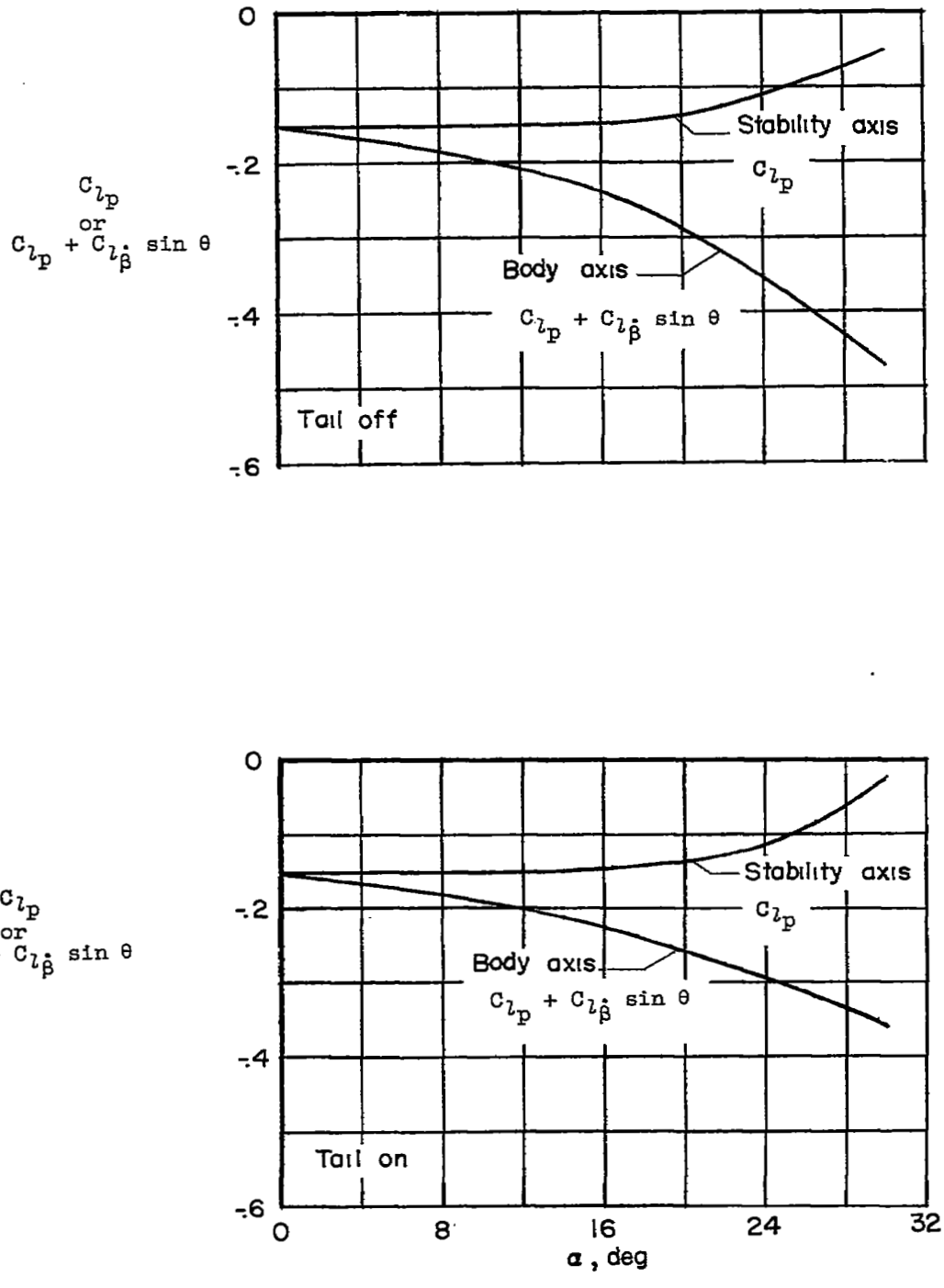

Figure 8.- Comparison of the damping-in-roll derivatives measured about the stability and body axes. Body-axis data from reference 1. $\delta_e = 0^\circ$.

LANGLEY RESEARCH CENTER
3 1176 00509 8026